Available online at www.sciencedirect.com

SciVerse ScienceDirect

Ceramics International 39 (2013) 6997–7005

CERAMICS INTERNATIONAL

www.elsevier.com/locate/ceramint

Characterisation of the pore-forming process in lightweight aggregate based on silica sludge by means of X-ray micro-tomography (micro-CT) and mercury intrusion porosimetry (MIP)

L. Korat[a], V. Ducman[a,*], A. Legat[a], B. Mirtič[b]

[a]ZAG Ljubljana, Dimičeva ul. 12, 1000 Ljubljana, Slovenia
[b]NTF, Aškerčeva c. 12, 1000 Ljubljana, Slovenia

Received 6 January 2013; received in revised form 7 February 2013; accepted 11 February 2013
Available online 27 February 2013

Abstract

In the case of lightweight aggregate (LWA), porosity can be achieved by means of a high temperature foaming process. During this process a glassy matrix is created, and almost simultaneously the added foaming agent degasses and the resulting gasses remain trapped inside the glassy structure. The present paper deals with the foaming process which occurs in the case of silica sludge to which fly ash, which creates liquid phase, has been added, as well as SiC, which acts as a foaming agent. The development of porosity within the structure of this material was investigated at different temperatures and dwelling times by means of X-ray micro-tomography (micro-CT), and mercury intrusion porosimetry (MIP). The results were compared by means of both X-ray micro-tomography and mercury intrusion porosimetry, the first technique being applied within the pore size distribution range of between 50 μm to more than 1 mm, and the second within the range, between 0.0055 and 360 μm. Both techniques have certain limitations as well as certain advantages, but in the case of the investigated system micro-CT gives much more reliable results about porosity development over a prolonged firing time, at the selected temperature. The results showed that, at the selected temperature, which in this case amounted to 1220 °C, porosity as well as median pore size increased with increased dwelling times. In the case of prolonged dwelling times, the number of pores decreased, but, on the other hand, the volume of these pores increased.

Keywords: B. Porosity; Lightweight aggregate; X-ray micro-tomography (micro-CT); Mercury intrusion porosimetry (MIP)

1. Introduction

Lightweight aggregate (LWA) is an aggregate with a maximum density of 2 g/cm^3 according to EN 13055-1:2002 [1]. Nowadays it represents a significant part of the total quantity of aggregates used in the construction industry, for two main reasons: (i) there is a decrease in the deadweight of structures, and (ii) there is an improvement in the thermal and/or acoustic insulation properties of structures made using LWA.

Expanded clay aggregate, which is produced by firing clay granules at 1000–1200 °C, so that the clay is expanded by gasses generated inside the mass, is mostly used. The density of the particles is usually within the range 400–800 kg/m^3 and the porosity is of the open type [2]. Lightweight glass aggregates usually have closed porosity, and are produced from glass by a foaming process [3]. In order to achieve proper expansion, the raw material has to contain components which release gas when decomposed, and it also needs to be sufficiently viscous (in its glassy state) at the gas formation temperature so that the gas remains trapped in the structure. That expansion or foaming of the material depends on the initial composition of the raw material, and on the firing temperature. Foaming agents can be selected from sulphides, carbonates, water-glass, Fe_2O_3, MnO_2, SiC etc [3–6]. These agents degas within the range between the softening point and the maximum firing temperature, and the resulting gasses remain trapped within the glassy structure. It should be noted that in recent years much effort has been invested in the finding of the best way to use different kinds of waste materials for the production of lightweight materials [7–14].

*Corresponding author. Tel.: +386 1 2804 438; fax: +386 1 2804 484.
E-mail address: vilma.ducman@zag.si (V. Ducman).

0272-8842/$ - see front matter © 2013 Elsevier Ltd and Techna Group S.r.l. All rights reserved.
http://dx.doi.org/10.1016/j.ceramint.2013.02.037

In all types of LWA, one of the most important parameters is porosity: overall porosity, pore size, close or open pores, thickness of the inner and outer walls. The development of porosity within the structure of the material depends on the following factors:

1. the supply of gas, which is the result of the chemical reaction and the heat flux,
2. the breaking of walls and coalescence,
3. the diffusion of small bubbles into larger ones due to the differences in pressure.

The first two factors predominate, whereas the third factor can be neglected due to the small size of the diffusion coefficient and the solubility in the liquid phase [3]. The growth of bubbles is shown schematically in Fig. 1.

Development of porosity can be observed by means of various two-dimensional and three-dimensional based techniques. X-ray micro-tomography is one such non-destructive technique which can be used for the characterisation of the material's microstructure. By means of a tomographic reconstruction of the projection images a 3D map of the X-ray absorption can be obtained. Because different material features and phases often have different X-ray absorption properties, such different features from these images can be easily identified. In the case of X-ray micro-tomography, the spatial resolution of 3D maps or images can approach 1 μm in three dimensions at a one-micron level of spatial resolution [15]. This technique is frequently used to determine the characteristics of different building materials, such as stones and concrete, in order to obtain data about the total porosity, the phase distribution, voids and cracks [16], as well as in the case of ceramic foams [17,18], or in the investigation of cement pastes in order to evaluate their geometrical and morphological characteristics [19]. In the case of porous materials, and if this three-dimensional technique is supported by means of a suitable programme for image analysis, walls, pores, and pore interconnectivity can be captured [20,21].

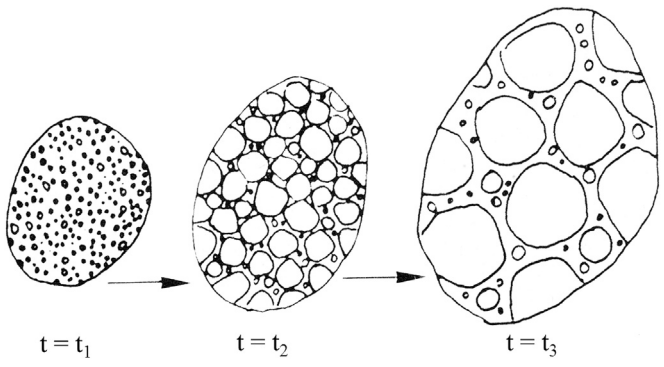

Fig. 1. Schematic diagram of the growth of bubbles inside a granule (after Köse and Bayer [3]).

Mercury intrusion porosimetry (MIP), too, can be used for the determination of pore size distribution. The latter can be determined from the volume of mercury which is intruded at each pressure increment, whereas total porosity is determined from the total intruded volume. The MIP technique is widely used to study the pore structure of materials with pore diameters ranging from 0.0055 to 360 μm. However, in the case of certain systems, e.g. in hydrated cement pastes [23,24] it has been shown that MIP measurements of pore size distribution systematically misallocates the sizes of almost all the volume of the pores, with an underestimation of the large pores and an overestimation of the small pores. It appears that the failure of the MIP method is, in the case of cement systems, intrinsic rather than accidental, and derives from the lack of direct accessibility of most of the pore volume (including air voids) to the mercury surrounding the specimen. Furthermore, in the case of highly porous structures, errors can also be made due to the breaking of the inner pore's walls, which then gives distorted results [25].

The objective of the investigations described in this paper is to present the evolution of porosity within the silica sludge–fly ash–SiC system, at elevated temperatures with different dwelling times. Comparative studies between results obtained by using this relatively new method, and those obtained by the more widely spread X-ray micro-tomography, as well as by established and well known mercury intrusion porosimetry, were performed.

2. Experimental

2.1. Preparation of the granules

The waste silica sludge which is left over after sand screening in quarries was used as the initial material. It contains a large amount of very fine silica sand (over 60%), as well as feldspar and clay. Silica sludge represented 50 wt% of the material, whereas 40 wt% of fly ash obtained from coal combustion was added, and 10 wt% of Fe_2O_3/SiC. Granules made from the above-described material were heated up to the selected temperatures using a heating rate of 10 °C/min. The dwelling times at the optimal temperature were: 0, 5, 10, 20 and 60 min.

2.2. Methods

2.2.1. DTA/TG

DTA/TG analysis of the foaming agent SiC was performed using a heating rate of 10 °C/min up to the maximum temperature of 1400 °C.

2.2.2. Hot stage microscope

The expansion process of the selected mixtures was observed by means of a hot-stage microscope, using a heating rate of 10 °C/min up to the maximum temperature of 1400 °C.

2.2.3. SEM microscopy

The microstructures of the fired granules were analysed using a JEOL 5500 LV scanning electron microscope (SEM) in low vacuum mode.

2.2.4. X-ray micro-tomography (micro-CT)

Tomographic scans were performed using an "Xradia 400" X-ray computed micro-tomograph on the fired granules. The X-ray energy was set to values of 80 kV and 125 μA, for all the samples. Using a high precision rotating stage, 1000 projection images were taken from different view-points (recorded at different angles during stepwise rotation between 0° and 360° around the vertical axis) with an exposure time of 5 s per projection. Beam hardening was reduced by the presence of an LE#1 filter (which improves the reconstructed image quality, by removing low-energy X-rays) between the source and the detector. The transmitted images were then detected by an X-ray image detector which consisted of a CCD camera equipped with a 0.39X magnification optical objective. The pixel resolution under these conditions was between 13 and 20 μm, depending on the sample. The tomographic reconstruction was performed using XMReconstructor software. Using the stack of slices obtained in this way it was possible to define the reconstructed volumetric data of the scanned object. Avizo Fire 3D-image analysis software was used for pore segmentation, object separation, quantification, and visualisation of the internal structure.

2.2.5. Mercury intrusion porosimetry (MIP)

Porosity and pore size distribution were determined on the whole granule, using a AutoPore IV 9510 Hg-porosimeter from Micromeritics, within a pressure range of up to 414 MPa. The fired granules were first scanned using micro-CT, and after this they were analysed using MIP.

3. Results and discussion

If a foaming process is to be successful, two main conditions have to be fulfilled:

- that a liquid phase is present, which depends on the chemical composition of the material as well as upon whether the temperature is high enough,
- that a foaming agent is present, which must decompose within the temperature range where the viscosity of the liquid is high enough to trap gasses within the structure.

3.1. Selection of the pore-forming agent and determination of the temperature of foaming

For the evaluation of suitability of potential pore-forming agents, two agents were selected, for which it was expected that they would decompose at a temperature near or above 1200 °C: Fe_2O_3, and SiC. The results are presented in Figs. 2 and 4, respectively.

It can be seen from Fig. 2 (the TG curve) that the decomposition of Fe_2O_3 starts at around 1400 °C, where the mass loss is 2.5%.

The sample with added Fe_2O_3 was also analysed using a hot stage microscope (Fig. 3). From Fig. 3 it can be seen that no foaming or bloating was present in the sample if Fe_2O_3 is added as a foaming agent; the melting point was determined to be at 1205 °C, and, as can be seen from Fig. 2, decomposition of the Fe_2O_3 took place at around 1400 °C. It was thus determined that the temperature of decomposition was not suitable for the investigated system, since it was too high.

When SiC was analysed in order to determine its temperature range of decomposition, it can be seen from the TG curve in Fig. 4 that decomposition of SiC starts at around 1200 °C, and is accompanied by a rise in weight since SiC reacts with oxygen from the atmosphere, and the following reaction takes

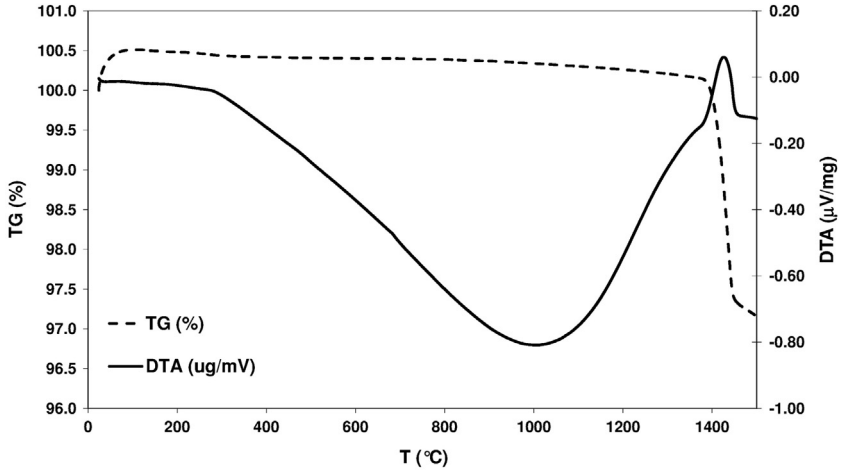

Fig. 2. DTA/TG examination of Fe_2O_3.

place [6]:

$$SiC + 2O_2 \rightarrow SiO_2 + CO_2 \quad (1)$$

When, instead of Fe_2O_3, SiC was used as the foaming agent, the analysis performed using the hot stage microscope confirmed that bloating/foaming was present in the selected system (Fig. 5). Previously (Fig. 3) it had been confirmed that the melting point of the investigated system was at 1205 °C, and that the decomposition of SiC starts gradually at around 1200 °C (Fig. 4). Both the processes take place simultaneously, so that gasses are trapped inside the glassy structure, resulting in a porous structure, which was confirmed by the hot stage microscope analysis (Figs. 5 and 6).

From Fig. 5 it is seen that the first dimensional changes are present at a temperature somewhat above 1200 °C, which is confirmed in Fig. 6, where the first signs of changes within the structure can be seen at 1230 °C, where the edges of the investigated sample became uneven. By the time the temperature reached to 1280 °C, the sample was bloated, whereas at 1380 °C the viscosity of glassy system was so high that gasses could not remain trapped in the system, the pressure of gases is too high, and the structure gradually collapses, which is clearly evident also from Fig. 5.

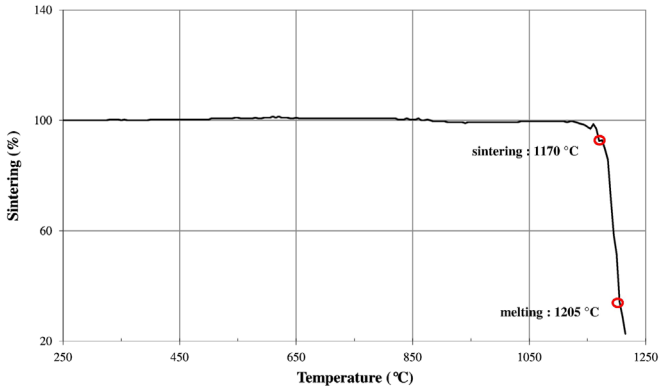

Fig. 3. Temperature range of foaming for the investigated mixture of silica mud, fly ash and Fe_2O_3.

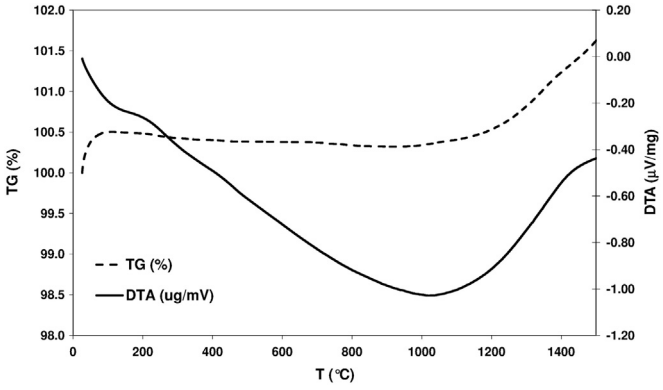

Fig. 4. DTA/TG examination of SiC.

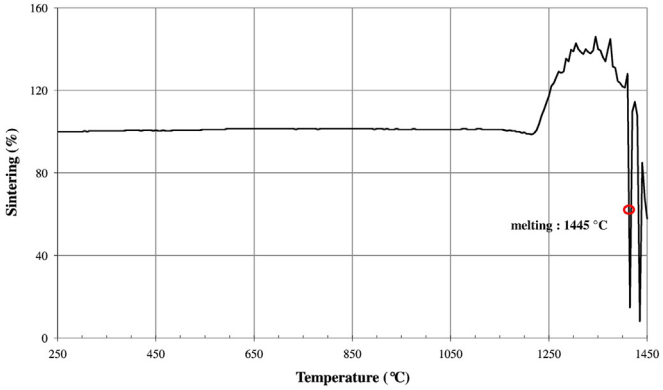

Fig. 5. Temperature range of foaming for the investigated mixture.

3.2. Microstructural investigations

Based on the findings presented in Section 3.1, granules with the addition of SiC were fired up to different temperatures with different dwelling times, and microstructural examinations were performed using micro-tomography and MIP. Granules of the investigated systems were fired up to different temperatures (1210, 1220, 1230, 1240, and 1250) and at the selected temperature of 1220 °C different dwelling times were applied (0, 5, 10, 20, and 60 min). The samples were designated as T0, T5, T10, T20, and T60, according to the corresponding dwelling times.

Firstly, optical and SEM analyses (Fig. 7) were performed in order to obtain qualitative information: the approximate size of the pores and the walls, and the presence of a liquid

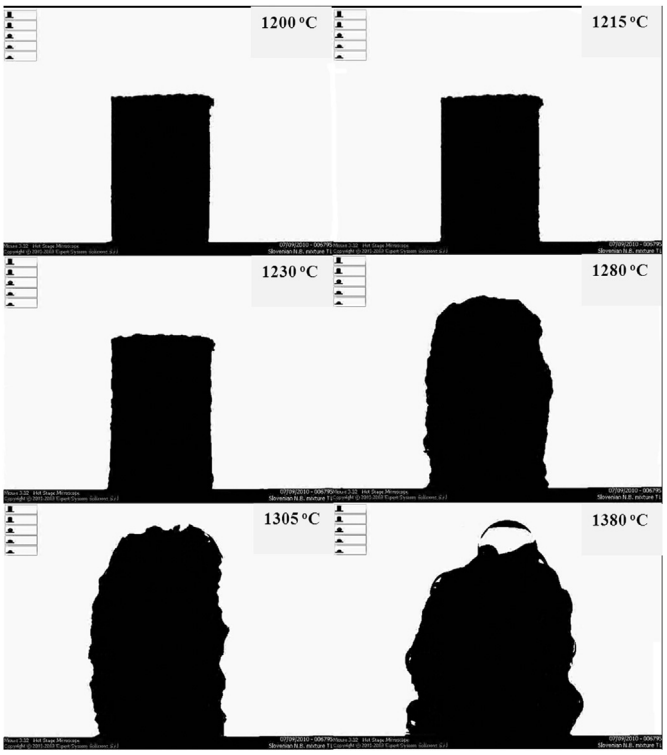

Fig. 6. Selected images from the hot stage microscope taken at 1200, 1215, 1230, 1280, 1305, and 1380 °C.

phase, which can be seen from the morphology (Fig. 7b).

Even if such an analysis is supported by a relevant image analysis programme, the information obtained from SEM or an optical microscope refers to just one cross section at a time, so that lot of cross sections have to be prepared and analysed in order to obtain an insight into the bulk (3D) features. On the other hand, if micro-CT analysis is used, much more information can be obtained in a shorter time, as well as, using appropriate computer software, good 3D data about the porosity.

From the results presented in Fig. 8 it is seen that the foaming process starts during the firing at a temperature of 1220 °C. Based on these results and those obtained using the hot stage microscope and DTA/TG analysis (Figs. 5 and 6, respectively), a temperature of 1220 °C was selected as being optimal for the present system. Microstructure development was followed by firing at this temperature, with dwelling times of 0, 5, 10, 20 and 60 min, which is presented in Fig. 9(a, d, g, j, and m). In this figure it can also be seen that the overall porosity, as well as the pore size distribution, depends on the time of exposure at the elevated temperature. At this temperature, in the case of a prolonged time there is a gas supply of CO_2 as a result of the chemical reaction of the decomposition of SiC, which then causes the breaking of walls and coalescence of smaller pores into bigger ones, as is presented schematically in Fig. 1.

Microstructural analysis of each of the fired granules using Avizo Fire 3D image analysing software was based firstly on the difference between the solid matrix and the air (inside the

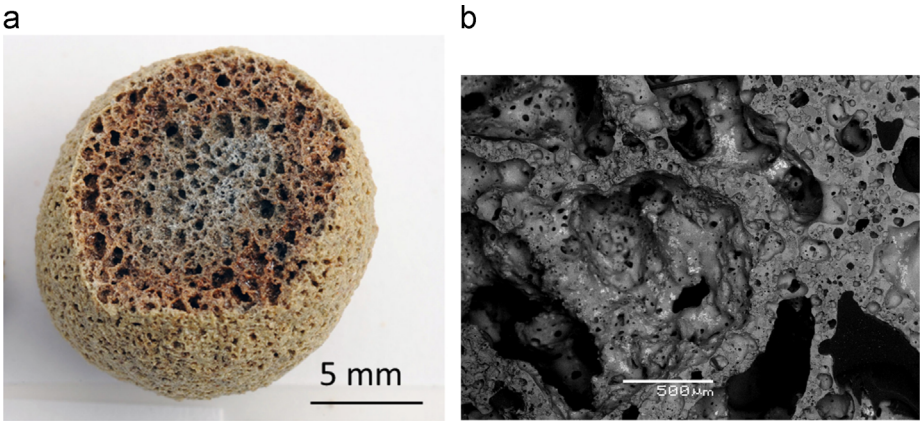

Fig. 7. (a) the appearance of a cross-section of the granules of sample T1, which was fired at 1220 °C for 20 min, and (b) the corresponding SEM image of the freshly broken sample.

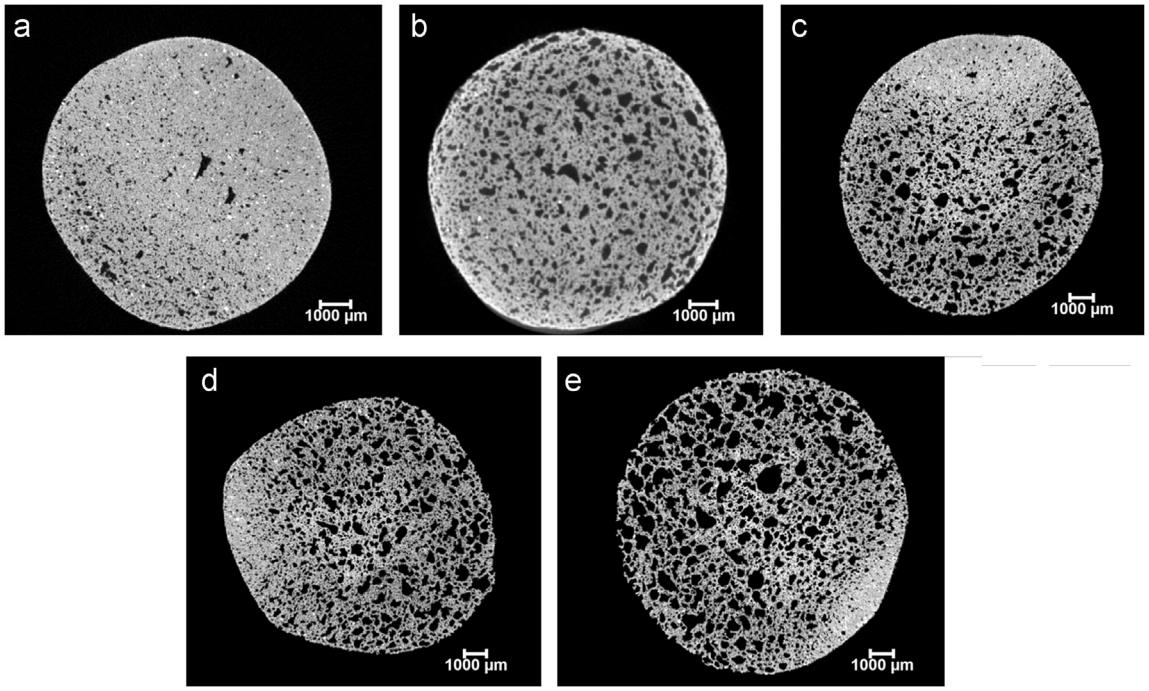

Fig. 8. YZ slice images (orthographic view) of samples fired at 1210 °C, 1220 °C, 1230 °C, 1240 °C and 1250 °C, with a dwelling time of 0 min.

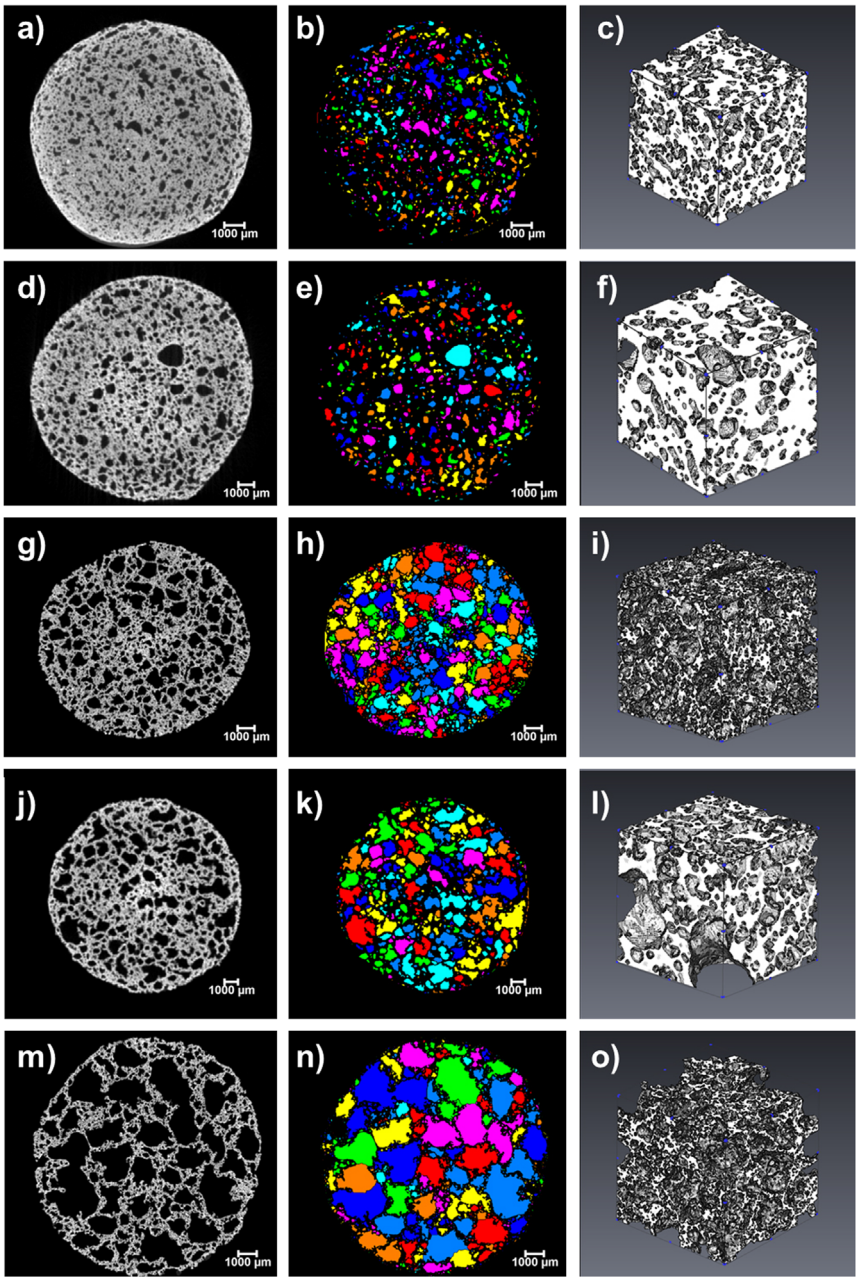

Fig. 9. YZ slice image (orthographic view) of samples fired at 1220 °C for 0, 5, 10, 20 and 60 min, (a, d, g, j, and m) grayscale images, (b, e, h, k, and n) 2D-images with labelled pores, (c, f, i, l, and o) 3D-pore shape of the material, the region of interest being approximately 1 mm in size.

pores and all around the solid matrix). In this study, all of the operations intended for the determination of porosity were performed on 3D slice views (planes, XZ, XY, and YZ). With appropriate image segmentation, which was based on hysteresis thresholding, the specimen was segmented from the voxel intensity histogram of the grayscale image. The white and black voxels represent the air and solid matrix, respectively. The objects with a low atomic number and a low density absorb fewer X-rays, resulting in bright areas (in our case, the solid matrix). Consequently, the higher the atomic number or density, the more X-rays are absorbed, creating darker regions [16]. After image segmentation, filling holes was applied to the material in order to ensure that any isolated black voxels (inside holes which were filled with air) were changed into white voxels as a solid matrix [17,22]. Using this operation, the pores were changed into a solid matrix, and also the outside boundaries of the pores of the fired granules which were connected with the surrounding air were determined. When the boundaries were set, a watershed algorithm [22,26] was applied to the binary images in order to separate the pores inside the fired granules. The term "watershed" comes from the analogy in which the grayscale image is treated as a topographic surface, i.e. the pixel (or voxel) intensity corresponds to the height of the point

Table 1
Overall porosity, share of pores and apparent porosity for the samples fired at 1220 °C for 0, 5, 10, 20 and 60 min, determined by using micro-CT and MIP.

Samples fired at 1220 °C for:	micro-CT						MIP
	Overall porosity in the range > 50 μm (%)	Share of pores within the range of pore size (%):					Apparent density (g/cm^3)
		50–100 μm	100–250 μm	250–500 μm	500–1000 μ	≥ 1000 μm	
0 min	16.6	1.73	16.21	27.59	50.82	3.66	1.23
5 min	19.4	0.27	4.06	6.30	52.05	37.33	0.99
10 min	53.4	0.13	0.33	1.61	40.85	57.09	0.90
20 min	46.4	0.09	0.64	0.63	6.98	91.66	0.81
60 min	58.6	0.32	0.61	2.18	8.50	88.39	0.78

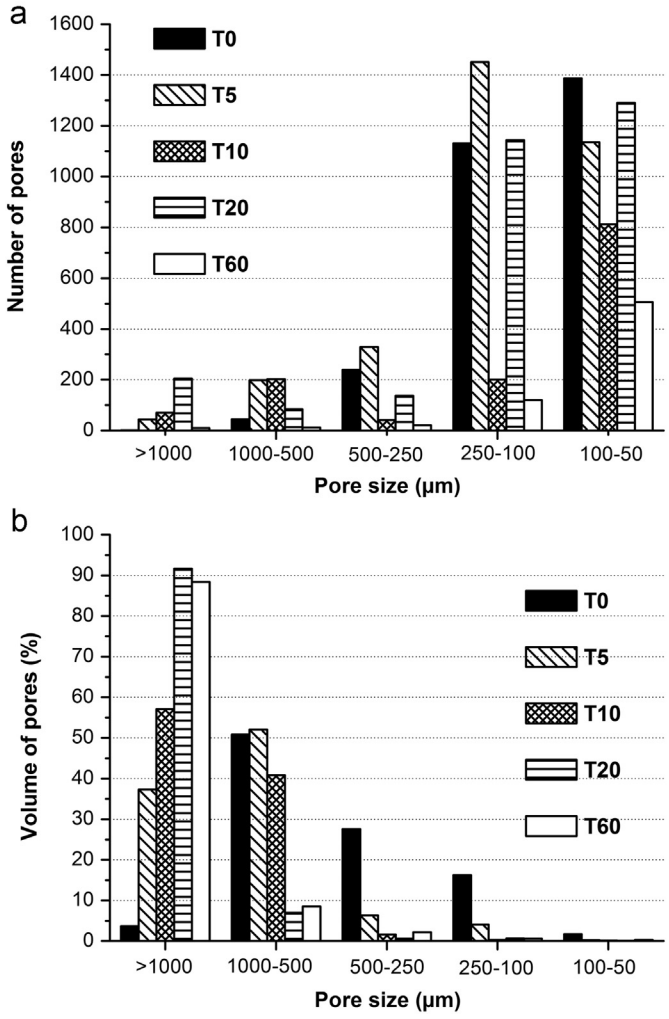

Fig. 10. Pore size distribution determined by means of micro-tomography for the samples fired at 1220 °C for 0, 5, 10, 20 and 60 min, presented as (a) the number of pores with regard to pore size, and (b) as the volume of pores with regard to pore size.

map. Once the separate pores have been identified, they can be labelled by different colours and further measured. Using a multiple labelling process, each pore can be identified in the label image, and assigned a unique index. Such labelled images are displayed by default using a cycling colour map (Fig. 9 b, e, h, k, and n). For better visualisation, Fig. 9 (c, f, i, l, and o) represents the 3D-pore shape of the material, the region of interest being approximately 1 mm in size, taken from the centre of the sample.

Using this method, the number of pores and the 3D volume were evaluated for each fired granule, and then summarised in Table 1. As expected, the overall porosity increased with the dwelling time (Table 1), as determined by both the methods, but micro-CT covers the pores above 50 μm whereas MIP covers the pore size range from 0.0055 to 360 μm. In the case of the micro-CT measurements, the porosity (taking into account pores bigger than 50 μm) increased from 16.6% to 58.6% after firing at 1220 °C with dwelling times of 0 and 60 min, respectively. It can be further seen that if the pore size distribution is presented as the "number of pores" versus the "pore size", then after firing for 10, 20 and, especially, 60 min, this number in the range of big pores over 250 μm is almost negligible (Fig. 10a); but if the distribution is presented as the "volume of pores" versus "pore size" (Fig. 10b) then the situation is the opposite, approximately 90% of the pore volume lies in the range above 250 μm (Table 1).

The results of MIP for the samples fired at 1220 °C are presented, for different dwelling times, in Fig. 11 and Table 1. MIP analysis was performed for all the samples in order to evaluate and compare the MIP results with those obtained from the micro-CT measurements. Based on the SEM figures (Fig. 7) it appears that many pores are closed, and that their sizes range up to 1 mm. As it is known that MIP is intended for measurements of open porosity, it is possible that the measurements would detect only open pores, so that the results would not be representative for the foaming process with closed pores, or that the mercury, under high pressure, breaks the pore wall and penetrates into otherwise closed pores. From the results of the MIP analysis (Table 1), it was confirmed that the apparent density, which is determined without mercury intrusion into the sample, and as such reliable enough, decreased from 1.23 to 0.78 g/cm^3. Further, from Fig. 11 it can be seen that, in all the samples, there is a bimodal pore size distribution: the first peak has its maximum between 0.1 and 1 μm, whereas the second peak is, in all cases, located above 10 μm, and up to 100 μm. With a prolonged dwelling time there is an increase in the number of pores in the

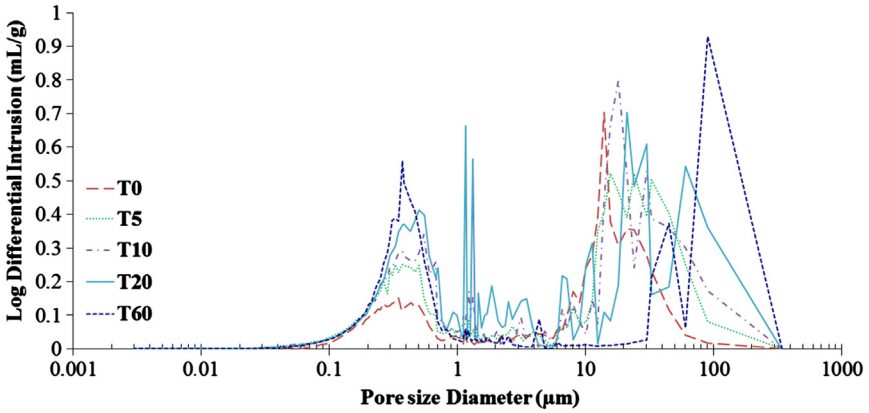

Fig. 11. Pore size distribution determined by means of MIP for the samples fired at 1220 °C for 0, 5, 10, 20 and 60 min.

lower and higher parts of the diagram. In the lower part the peaks remain in almost the same position, only their heights are different, which means that the average pore size in the lower part remains the same, but, in the case of the prolonged dwelling time, the porosity in this range is higher. The peaks in the upper range also show a shift of the maximum to higher values; for example, after firing for 10 min the second peak is around 20 μm, whereas after firing for 60 min the second peak reaches its maximum at 100 μm.

Despite the differences and to some extent distorted results obtained by MIP in the case of the investigated system, both the methods showed the same trends of pore growth. In the case of MIP, however, only smaller share of pores were detected in the range above 500 μm, although the micro-CT results show that the share of pores with sizes greater than 500 μm was, except in the case of T0, above 90%. This confirms the finding [23–25] that MIP underestimates the share of bigger pores either due to the bottleneck effect or due to the breaking of pore walls; therefore the porosity measured in such test is more related to the total porosity than to the open porosity [25].

Comparing the results of MIP and micro-CT, it has to be concluded that micro-CT seems to be more appropriate methodology for the study of LWA microstructure, even though it does not cover submicron sizes. Comparing the results presented in Fig. 7 and Table 1 (the share of pores with sizes above 50 μm), and MIP analysis, it appears very likely that MIP results distorted LWA pore size distributions (shifted to lower values).

4. Conclusions

A pore-forming process was successfully performed with a silica sludge, fly ash and SiC system, where fly ash contributed to the creation of the liquid phase and SiC acted as a foaming agent which decomposes at an elevated temperature, in our case at 1220 °C, so that gasses remain trapped in the structure, creating porosity. Evaluation of porosity was monitored by means of micro-CT and MIP.

In the case of both types of measurements (micro-CT and MIP) it was observed, as was expected, the results from both types of experiments in general showed higher values of porosity in the case of samples with prolonged dwelling times. Also, a large proportion of small pores was observed in the case of the samples with minimum dwelling times. With the prolongation of dwelling times, the number of pores decreased, but, on the other hand, the volume of those pores increased, which supports the theory of bubble growth of the bubble which is presented in Fig. 1.

MIP underestimates the share of bigger pores either due to the bottleneck effect or due to the breaking of pore walls. However, because it does not interfere with or destruct the sample, Micro-CT seems to be an appropriate methodology for the study of LWA microstructure, and it provides more reliable results then MIP. Last but not least, it is also worth noting that micro-CT provides much wider possibilities for the graphic presentations of the results.

Acknowledgements

This work has been financially supported by the Slovenian Research Agency (ARRS).The support of Mr. Robert Steine is hereby gratefully acknowledged.

References

[1] EN 13055-1:2002/AC:2004: Lightweight aggregates—Part 1: Lightweight aggregates for concrete, mortar and grout, 36 p.
[2] T.W., Bremner, J.P., Ries, W.H., Wolf, Environmental friendly uses of lightweight aggregates, V.M. Malhotra, K. Sakai (Eds.), in: Proceedings of the International Sustainable Development of Cement, Concrete and Concrete Structures, October 5–7 2005, pp. 201–210.
[3] S. Köse, G. Bayer, Schaumbildung im system Altglas–SiC und die Eigenschaften derartiger Schaumgläser, Glastechnik Ber 55 (7) (1982) 151–160.
[4] V. Ducman, Foaming process of waste glass using $CaCO_3$, MnO_2 and water–glass as foaming agents, in: C. Limbachiya, J. Roberts (Eds.), Sustainable Waste Management and Recycling, Glass Waste, Thomas Telford, London, 2004, pp. 59–66.
[5] E. Bernardo, G. Scarinci, S. Hreglich, Foam glass as a way of recycling glasses from cathode ray tubes, Glass Science and Technology 78 (1) (2005) 7–11.

[6] E. Bernardo, R. Cedro, M. Florean, S. Hreglich, Reutilization and stabilization of wastes by the production of glass foams, Ceramics International 33 (2007) 963–968.
[7] K.Y. Show, D.J. Lee, J.H. Tay, S.Y. Hong, C.Y. Chien, Lightweight aggregate from industrial sludge–marine clay mixes, Journal of Environmental Engineering 131 (7) (2005) 1106–1113.
[8] K.S. Wang, I.J. Chiou, H. Ching, D. Wang, Lightweight properties and pore structure of foamed material made from sewage sludge ash, Construction and Building Materials 19 (2005) 627–633.
[9] S.C. Huang, F.C. Chang, S.L. Lo, M.Y. Lee, C.F. Wang, J.D. Lin, Production of lightweight aggregate from mining residue, heavy metal sludge, and incinerator fly ash, Journal of Hazardous Materials 144 (2007) 52–58.
[10] K.J. Mun, Development and tests of lightweight aggregate using sewage sludge for non-structural concrete, Construction and Building Materials 21 (2007) 1583–1588.
[11] I.M. Anagnostopoulos, V.E. Stivanakis, Utilization of lignite power generation residue from the production of lightweight aggregate, Journal of Hazardous Materials 163 (2009) 329–336.
[12] B.G. Corrochano, J.A. Azcarate, M. Rodas, Characterisation of lightweight aggregates manufactured from washing aggregate sludge and fly ash, Resources, Conservation and Recycling 53 (10) (2009) 571–581.
[13] H.J. Chen, S.Y. Wang, C.W. Tang, Reuse of incineration fly ashes and reaction ashes for manufacturing lightweight aggregate, Construction and Building Materials 24 (2010) 46–55.
[14] C.L. Hwang, L.A.T. Bui, K.L. Lin, C.T. Lo, Manufacture and performance of lightweight aggregate from municipal solid waste incinerator fly ash and reservoir sediment for self-consolidating lightweight concrete, Cement and Concrete Composites 34 (10) (2012) 1159–1166.
[15] E.N. Landis, D.T. Keane, X-ray microtomography, Materials Characterisation 61 (2010) 1305–1316.
[16] V. Cnudde, A. Cwirzen, B. Masschaele, P.J.S. Jacobs, Porosity and microstructure characterisation of building stones and concretes, Engineering Geology 103 (2009) 76–83.
[17] E. Maire, P. Paolo Colombo, J. Adrien, L. Babout, L. Biasetto, Characterisation of the morphology of cellular ceramics by 3D image processing of X-ray tomography, Journal of the European Ceramic Society 27 (2007) 1973–1981.
[18] J. Luyten, S. Mullens, J. Cooymans, A.M. De Wilde, I. Thijs, R. Kemps, Different methods to synthesize ceramic foams, Journal of the European Ceramic Society 29 (2009) 829–832.
[19] E. Gallucci, K. Scrivener, A. Groso, M. Stampanoni, G. Margaritondo, 3D experimental investigation of the microstructure of cement pastes using synchrotron X-ray microtomography (μCT), Cement and Concrete Research 37 (2007) 360–368.
[20] R.C. Atwood, J.R. Jones, P.D. Lee, L.L. Hench, Analysis of pore interconnectivity in bioactive glass foams using X-ray microtomography, Scripta Materialia 51 (2004) 1029–1033.
[21] B. Maruyama, J.E. Spowart, D.J. Hooper, H.M. Mullens, A.M. Druma, C. Druma, M.K. Alam, A new technique for obtaining three-dimensional structures in pitch-based carbon foams, Scripta Materialia 54 (2006) 1709–1713.
[22] M.A.B., Promentilla, T., Sugiyama, K., Shimura, Three dimensional characterisation of air void system in cement-based materials, in: Proceedings of the 3rd International Conference—AC/VCA, 2008, pp. 940–947.
[23] S. Diamond, Mercury porosimetry; an inappropriate method for the measurement of pore size distributions in cement-based materials, Cement and Concrete Research 30 (2000) 1517–1525.
[24] J. Zhou, G. Ye, K. Breugel, Characterisation of pore structure in cement-based materials using pressurization–depressurization cycling mercury intrusion porosimetry (PDC-MIP), Cement and Concrete Research 40 (2010) 1120–1128.
[25] J.A. Bogas, A. Mauricio, M.F.C. Pereira, Microstructural analysis of Iberian expanded clay aggregates, Microscopy and Microanalysis 18 (5) (2012) 1190–1208.
[26] L. Vincent, P. Soille, watersheds in digital spaces: an efficient algorithm based on immersion simulations, IEEE Transactions on Pattern Analysis and Machine Intelligence 13 (1991) 583–585.